J. Fluid Mech. (1981), *vol.* 103, *pp.* 65–85
Printed in Great Britain

The distribution of convection velocities in turbulent pipe flow

By P. J. McCONACHIE

Department of Mechanical Engineering, University of Queensland, Brisbane, Australia

(Received 5 July 1979 and 14 April 1980)

The structure of fully developed turbulence in a smooth circular tube has been studied for a Reynolds number of 69000 (based on centre-line velocity and radius) and at a distance from the wall of $y^+ = 70$. The data were taken as correlations of the longitudinal component of turbulence in narrow frequency bands, the longitudinal and transverse separations being varied simultaneously. Fourier transformation of these correlations defines power spectral density functions with frequency ω and longitudinal and transverse wavenumbers k_x and k_z as the independent variables. In this form the data show the distribution of convection velocity among waves of different size and inclination as well as defining the coherence lengths associated with such wave packets.

Essential features of a geometrically similar wave description of the turbulence are discussed, such a model allowing considerable simplification in the description of the turbulence both for two-point and three-point space–time correlations of the velocity field. Morrison & Kronauer (1969) predicted that the wave convection velocity should depend only on total wavenumber k in a specific manner related to the mean velocity profile. The experimentally determined convection velocities contradict this prediction. An alternative formulation for convection velocity involving an additional empirical function of frequency $S(\omega)$, fits the data for the range of experimentation. Unfortunately the results provide no information on the functional dependence (if any) of convection velocity on distance from the wall.

1. Introduction

Significant effort has been devoted to determining the structure of fully developed turbulence by spatial and temporal correlations of the velocity and wall pressure fields. Townsend (1956), using a few two-point spatial correlations of the longitudinal velocity fluctuation, postulated a set of attached eddies capable of absorbing energy from the mean motion, while dissipating most of their energy in the sublayer. Townsend (1958) later modified this theory to comply with the measurements of Grant (1958). Favre, Gaviglio & Dumas (1957, 1958) made measurements of space–time correlations in a turbulent boundary layer and reasonably extensive results for the longitudinal velocity correlation $R_{11}(x, y, z, \tau_M)$ – with optimum time delay τ_M – are presented as contour maps in the x, y and y, z planes. In the Cartesian co-ordinates chosen x, y and z represent the relative separation of the measuring points in directions parallel to the outer flow, normal to the wall and transverse to the outer flow respectively. However, the elimination of the effect of convection velocity, presumably the

0022-1120/81/4605-3360 $02.00

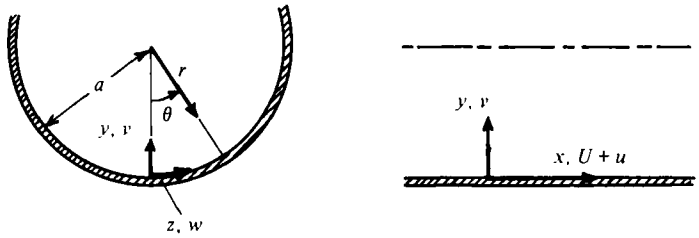

FIGURE 1. Pipe co-ordinates and velocity components. $y = a-r, z = a\theta$.

reason for introducing τ_M, makes it difficult to visualize the results in terms of a flow structure.

Bull (1967) sought information on the wall-pressure fluctuations through space–time correlations in broad and narrow frequency bands. He demonstrated that the wall-pressure correlations may be collapsed on to a single curve – which agrees with the structural similarity found in the measurements of Morrison & Kronauer (1969) for longitudinal turbulence data. Elliott (1972) measured static pressure and velocity fluctuations in an atmospheric boundary layer, the results indicating significant coherence in velocity fluctuations with separation from the boundary. Important sections of these results also confirm predictions expected from Morrison & Kronauer's (1969) work. Bullock, Cooper & Abernathy (1978) demonstrate that low-frequency, large-scale turbulence fluctuations extend over the majority of the radial region and that these components are highly correlated over large radial separations. By using a similarity variable $k_x y$, along with a normalized wall distance y/y_{ref}, both the Covariant and Quadrature narrow frequency band correlations of the longitudinal velocity fluctuations were shown to collapse.

Fully developed turbulence in a smooth circular tube, while representing one of the simplest cases of shear-flow turbulence, is difficult to completely quantify experimentally. Description of the turbulent velocity field by two-point space–time correlations requires six functions of five arguments each. The dependent variables are the three velocity components which have six pair combinations. Assuming the correlations are stationary in the x, z and t variables (defined in figure 1) these five arguments are: x_1-x_2, z_1-z_2, t_1-t_2, y_1 and y_2. Studies of the energy exchange mechanism by three-point space–time correlations would require 10 functions (triple combinations of the three velocity components) in nine arguments. The difficulty of experimentally determining and interpreting such a plethora of data prompts one to seek ways of reducing the dimensionality of the flow description.

Fourier transformation of the correlations in the stationary arguments x_1-x_2, z_1-z_2, and t_1-t_2 will yield spectral functions with the corresponding transform arguments k_x, k_z and ω. As the correlations are of relatively small extent transversely (about one radian) the use of a Fourier transform in place of a Fourier series expansion is permissible and is used throughout this paper. Non-stationarity in the y co-ordinate prohibits Fourier transformation, although an eigenfunction expansion can be effected (Lumley 1967). Correlation functions and power density functions are conjugate forms of the same data and we can validly consider either representation, i.e. $R_{ij}(\Delta x, \Delta z, \Delta t, y_1, y_2)$ or $\Phi_{ij}(k_x, k_z, \omega, y_1, y_2)$. A spectral representation *per se* involves no simplification in the flow description.

However a considerable simplification is possible if the flow can be represented by a collection of geometrically similar Tollmien–Schlichting-type waves. Such an approach is outlined by Morrison & Kronauer (1969) and will be considered in more detail for the remainder of this paper. No claim is made from the present data that the flow is composed physically of geometrically similar waves – a standpoint quite validly questioned by Kovasznay, Kibens & Blackwelder (1970), who point out that a spectral approach is not the only possible transformation of the space–time correlations. Nevertheless, even with this limitation in mind, it is believed that pipe turbulence can be most economically represented by a geometrically similar wave model and furthermore the present data do not conflict with such a hypothesis.

2. Proposed wave model

The concept of geometric similarity applied to the constant stress region of the turbulent boundary layer is both well established and well illustrated by Townsend (1976). Using arguments based on the formation of Reynolds stress and energy dissipation scale he postulates the flow to be composed of persistent organized flow patterns which extend to the wall. These attached eddies have diameters proportional to the distance of their centres from the wall and are geometrically similar in their velocity distributions – although no constraint is placed on the variation of a particular eddy centre in the streamwise direction.

A wave model, of the type first proposed by Morrison & Kronauer (1969) is a particular case of geometric similarity in which the proportions of a particular disturbance are invariant in the stream-wise direction but the amplitude fluctuates with energy exchange to or from this disturbance. Convection velocity is constrained to be invariant in the co-ordinate y defining distance from the wall – thus guaranteeing no distortion of the disturbance in the streamwise direction.

Following the work of Morrison & Kronauer (1969) we consider the flow as being composed of two-dimensional waves ($\partial/\partial\hat{x} = 0$) of the type shown in figure 2. For a component of wavenumber k and inclination α the following equations represent the velocity fluctuations in the co-ordinate system $(\hat{x}, y, \hat{z})$ with $\hat{z}$ oriented in the direction of wave propagation:

$$\left.\begin{aligned} \hat{u}(t,k,\alpha) &= A(t,k,\alpha)\,\mathscr{R}[h_2(ky,\alpha)\exp(jk(\hat{z}-C(k,\alpha).t))],\\ v(t,k,\alpha) &= A(t,k,\alpha)\,\mathscr{R}[-jh_1(ky,\alpha)\exp(jk(\hat{z}-C(k,\alpha).t))] = -\psi_{\hat{z}},\\ \hat{w}(t,k,\alpha) &= A(t,k,\alpha)\,\mathscr{R}[h_1'(ky,\alpha)\exp(jk(\hat{z}-C(k,\alpha).t))] = \psi_y. \end{aligned}\right\} \tag{1}$$

On satisfying the continuity equation we have $v_y + \hat{w}_{\hat{z}} = 0$. The velocities $\hat{u}$, v, $\hat{w}$ are actually functions of five arguments, viz. t, k, α, y, $\hat{z}$; however, for convenience the functional dependence on y and $\hat{z}$ is suppressed in (1) and in the subsequent text. Henceforth the real parts are taken to represent physical quantities and the prime denotes differentiation of the complex functions h_1 and h_2 with respect to ky, the scaling variable.

Such a wave will induce velocity fluctuations in the co-ordinate directions x and z given by

$$\left.\begin{aligned} u(t,k,\alpha) &= \hat{u}(t,k,\alpha)\cos\alpha + \hat{w}(t,k,\alpha)\sin\alpha,\\ w(t,k,\alpha) &= \hat{u}(t,k,\alpha)\sin\alpha + \hat{w}(t,k,\alpha)\cos\alpha, \end{aligned}\right\} \tag{2}$$

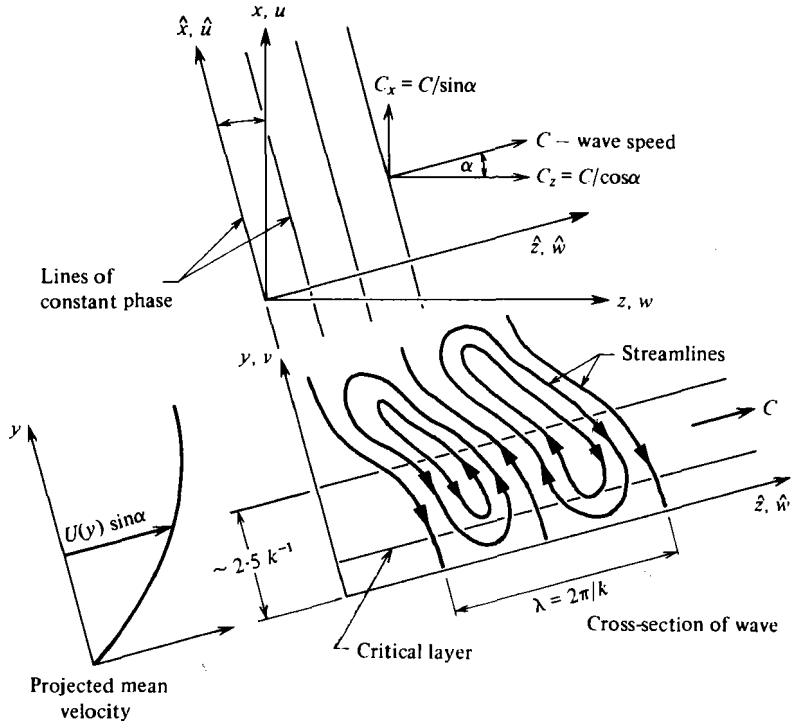

FIGURE 2. Wave schematic diagram. $k_x = k\sin\alpha$, $k_z = k\cos\alpha$, $\omega^+ = C_x^+ k_x^+ = C^+ k^+$.

while the total longitudinal velocity fluctuation $u(t)$ is

$$u(t) = \int_0^\infty dk \int_{-\frac{1}{2}\pi}^{\frac{1}{2}\pi} d\alpha\, u(t, k, \alpha), \tag{3}$$

similar equations applying to the components $v(t)$ and $w(t)$.

For each component wave in the flow, the three velocity components $u(t, k, \alpha)$, $v(t, k, \alpha)$ and $w(t, k, \alpha)$ are instantaneously related, although their magnitude is constantly varying due to energy exchange with other waves in the flow. This varying magnitude for each component wave is manifested in an apparent spread of convection velocities (or wave frequencies $\omega = kC(k, \alpha)$), as the three-dimensional spectral density function of the longitudinal velocity illustrates:

$$\Phi_{uu}(\omega, k, \alpha) = 0{\cdot}5\,|h_2\cos\alpha + h_1'\sin\alpha|^2\,\Phi_{AA}(\zeta, k, \alpha). \tag{4}$$

Here $\omega_0 = k\,.\,C(k, \alpha)$, $\zeta = \omega - \omega_0$ and $\Phi_{AA}(\zeta, k, \alpha)$ is the frequency spectrum of the amplitude term $A(t, k, \alpha)$. Equation (4) is obtained by first determining the complex Fourier transform of the random velocity fluctuation $u(t, k, \alpha)$ thus allowing the direct computation of $\Phi_{uu}(\omega, k, \alpha)$. In this formulation $\Phi_{uu}(\omega, k, \alpha)$ is assumed to exist only for positive ω while $\Phi_{AA}(\zeta, k, \alpha)$ is defined for both positive and negative ζ. Zero energy exchange to or from a wave ($A(t, k, \alpha) =$ a constant) implies an infinitesimal spectral spread in ω and corresponds to a wave of infinite extent in the direction of propagation. It is the spread in convection velocities which demonstrates energy exchange between component modes of the flow.

If the turbulence can be considered as composed of geometrically similar waves, as postulated in (1), considerable simplification in the flow description is possible. All the two point space–time properties are represented by the functions $h_1(ky, \alpha)$, $h_2(ky, \alpha)$, $C(k, \alpha)$ and $\Phi_{AA}(\zeta, k, \alpha)$ instead of the original six correlation functions (of five arguments each) as required by the unmodified space–time correlation description. Studies of the energy exchange mechanism by three-point space–time correlations would require 10 functions (triple combinations of the three velocity components) in nine arguments. With the geometrically similar wave model proposed, description of the energy exchange mechanism is provided by the single three point spectral function $\Phi_{AAA}(\zeta_1, \zeta_2, k_1, k_2, \alpha_1, \alpha_2)$ alone.

Several tests may be designed to check the applicability of a geometrically similar wave model. Firstly, is there a unique relationship between circular frequency and the wave inclination and wavenumber irrespective of distance from the wall? This is equivalent to requiring that $C(k, \alpha)$ and $\Phi_{AA}(\zeta, k, \alpha)$ be independent of y throughout the flow. Secondly, is there a significant degree of co-ordination for any of the three fluctuating velocity components in the direction normal to the wall? Thirdly, are the statistical properties of $A(t, k, \alpha)$ such as to make a wave model representation physically useful in quantifying the turbulence?

The work of Bullock *et al.* (1978) indicates that the large-scale fluctuations are highly correlated radially and scale on a similarity variable $k_x y$ (along with a normalized wall distance y/y_{ref}). These results indicate that the second condition is capable of being satisfied, however further experiments with varied distances from the wall and other velocity components are being conducted to establish these first two conditions more closely.

Determination of the wave parameters $C(k, \alpha)$ and $\Phi_{AA}(\zeta, k, \alpha)$ is possible by considering the three-dimensional power spectral density function of the longitudinal velocity $\Phi_{uu}(\omega, k_x, k_z)$ defined from the series of correlations in narrow frequency bands formed by varying the longitudinal and transverse spacings jointly at a fixed distance from the wall. This technique is further described in § 4, with (8) and (9) providing the functional relationships between filtered spatial correlations and their associated spectral density functions. The investigations of Morrison & Kronauer (1969) and later Morrison, Bullock & Kronauer (1971) considered only those correlations formed by variation of longitudinal spacing at zero transverse separation and vice versa. Integral projections of $\Phi_{uu}(\omega, k_x, k_z)$ on to the $k_x = 0$ and $k_z = 0$ planes produced $\Phi_{uu}(\omega, k_z)$ and $\Phi_{uu}(\omega, k_x)$ respectively. These results indicate that, for any wave frequency ω, the transverse wavenumbers k_z are of much greater extent than their longitudinal counterparts k_x. Furthermore as the spectral function $\Phi_{uu}(\omega, k_x)$ represents the integral projection of $\Phi_{uu}(\omega, k_x, k_z)$ onto the plane $k_z = 0$, it is extremely likely that a cross-section through $\Phi_{uu}(\omega, k_x, k_z)$ at any transverse wavenumber will be much narrower than indicated by $\Phi_{uu}(\omega, k_x)$. Provided that this extent is not significantly greater than the results of Morrison & Kronauer (1969) a wave model representation would appear to be useful and the third criterion outlined above will be satisfied. The physical significance of this wavenumber spread will be discussed in the following section – this paper being concerned predominantly with determining the form of the wave parameters $C(k, \alpha)$ and $\Phi_{AA}(\zeta, k, \alpha)$.

The power spectral density function $\Phi_{uu}(\omega, k_x, k_z)$ is real and unchanged if the signs of all three arguments are reversed. Further, since the time-averaged flow is free from

swirl, the correlations are symmetric in transverse spacing resulting in an even power spectral density function in k_z. If for convenience k_x is always considered positive, the three-dimensional spectral density is composed of two parts, $\Phi_{uu}(\omega, k_x, k_z)$ and $\Phi_{uu}(-\omega, k_x, k_z)$, the former being associated with waves propagating against the mean-flow direction, while the latter corresponds to waves propagating downstream with the flow. Morrison & Kronauer (1969) interpreted the data of Favre *et al.* (1958) and Willmarth & Woolridge (1962) to indicate negligible upstream propagation. While this approach seems justified some estimate of the percentage of upstream propagation would be desirable.

3. Significance of wave parameters $C(k, \alpha)$ and $\Phi_{AA}(\zeta, k, \alpha)$

Considerations of the energy exchange between component waves has been shown to produce a spectral spread in ω for any fixed wavenumber and inclination. Equation (4) can be expressed more generally as the cross-spectral density function between velocity fluctuations in any of the co-ordinate x, y and z, viz.

$$\Phi_{ij}(\omega, k, \alpha) = f_{ij}(ky, \alpha)\, \Phi_{AA}(\zeta, k, \alpha), \tag{5}$$

where $f_{ij}(ky, \alpha)$ and $\Phi_{ij}(\omega, k, \alpha)$ are complex for $i \neq j$. Hence $C(k, \alpha)$, $\Phi_{AA}(\zeta, k, \alpha)$ can be determined experimentally by selecting any velocity component pair. For convenience $\Phi_{uu}(\omega, k_x, k_z)$ has been measured.

Consider a very narrow hypothetical spatial filter selecting a single component of wavenumber k and inclination α out of any velocity component. Depending on the behaviour of the amplitude term $A(t, k, \alpha)$ the observed velocity component would exhibit varying periods of coherence. If $A(t, k, \alpha)$ is varying slowly in time, the velocity component observed will be coherent over long time intervals, while rapid variation in $A(t, k, \alpha)$ will be associated with short coherence times. An estimate of the lower bound for the observed coherence times is provided by the inverse of the half bandwidth, B_ω of either $\Phi_{uu}(\omega, k, \alpha)$ or $\Phi_{AA}(\zeta, k, \alpha)$. Similarly if one considered the time auto-correlation of the spatially filtered velocity component the decay rate of the basic oscillation (frequency $\omega_0 = k\, C(k, \alpha)$) would be proportional to B_ω^{-1}. It must be stressed that the coherence time B_ω^{-1} is a lower bound to the coherence time – that is, it is possible for individual members of the ensemble to have much larger coherence times than that of the ensemble. An alternative way of considering the frequency spread (fixed k and α) is to associate this with a spread in convection velocity.

Similarly if one used a very narrow temporal filter to select a particular frequency ω, then a spread of wavenumbers and inclinations would be observed. For waves of fixed inclination, the inverse of the half bandwidth of the wavenumber spread B_k^{-1} will provide a lower bound for the coherence length. Coherence time (B_ω^{-1}) and coherence length (B_k^{-1}), at fixed inclinations are related through the convection velocity $C(k, \alpha)$ and simply provide complimentary ways of describing the amplitude term $\Phi_{AA}(\zeta, k, \alpha)$.

Pipe turbulence is characterized by a thin layer near the wall where viscosity plays an important role, while in the bulk of the flow (where the mean velocity profile is logarithmic) the phenomena are essentially inviscid (Laufer (1954)). Morrison & Kronauer (1969) consider a logarithmic mean velocity profile (with complex functions h_1 and h_2 assumed independent of wave inclination) and consider the Navier–Stokes

equations for a particular wave. For the Reynolds numbers of interest they presume that the viscid terms are small and rewrite the equations as linear inviscid terms and nonlinear terms representing forcing functions for the linear inviscid terms. To ensure that the linear inviscid terms are independent of absolute scale k, they postulate that the wave speed $C(k)$ matches the mean velocity component (projected into the wave cross-section) at a distance y_c from the wall such that ky_c is constant ($\beta = ky_c$) – or alternatively the critical layer is also geometrically scaled for all wave sizes. For the pipe flow considered the longitudinal convection velocity $C_x(k)$ is expressed by

$$C_x^+(k) = 5{\cdot}5 + 5{\cdot}75 \log_{10}(\beta/k^+), \tag{6}$$

for the simple case of h_1 and h_2 independent of wave inclination and waves of extent large compared with the thickness of the wall layer ($y^+ < 70$).

If this postulate of Morrison & Kronauer (1969) is correct and the critical layer scales geometrically on wave size then it is sufficient to check (6) for a single distance from the wall and several wave sizes k^+ to determine if a geometrically similar wave model is applicable to pipe turbulence. Should the convection velocity results at a single y^+ disagree with (6) then either the concept of a geometrically scaled critical layer is wrong or the wave model postulated is incorrect with convection velocity dependent on distance from the wall y^+.

Obviously the best experimental strategy is to attempt to verify (6) at a single y^+ before proceeding to the enormous task of measuring convection velocities at different distances from the wall.

4. Experimental determination of wave spectra

Filtered spatial correlations were measured in a 13·34 cm diameter extruded aluminium tube fitted with a traversing mechanism and probes as described by McConachie (1975). By use of a special flange arrangement, the final 64 cm section of pipe was removed and a Rank–Taylor alignment telescope placed within 13 cm of the probes thus enabling the distance from the wall to be set accurately to within 12·5 μm. Wire parallelism and the positions of zero longitudinal and transverse separation were determined by placing a small optical mirror, angled at 45°, under the two probes and viewing their images with the alignment telescope. Because of the location and construction of the flange and associated tailpiece, no interference to the flow was expected. Leakage of air from the longitudinal and transverse slots in the pipe wall was prevented by the use of appropriate length epoxy sections (fitting flush with the pipe wall) inserted into the unused portions of these slots. Over the longitudinal range used, the variation in wall profile was within 25 μm while a variation of 90 μm transversely was symptotic of slight pipe ovality. Such variations, occurring as they do in regions of low correlation (and hence highest statistical uncertainty) have negligible effect on the measured results. At maximum longitudinal separation the forward probe was 63·5 diameters (8·48 metres) downstream of the pipe inlet section and entry screen.

Measurement conditions were chosen as follows. From the experiments of Morrison & Kronauer (1969) it would appear that the waves are distributed more or less uniformly over a range bounded at one extreme by the largest waves which the tube can contain ($k^+_{\min} \approx 2\pi/a^+$ or $\lambda^+_{\max} \approx a^+$) and at the other extreme by the smallest

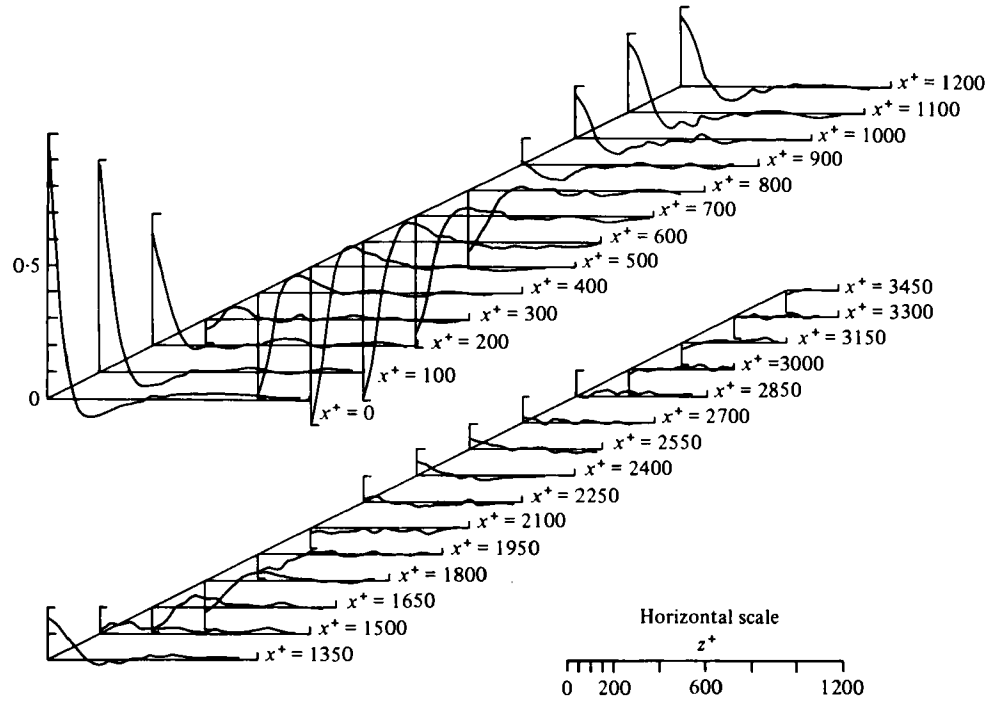

FIGURE 3. Two-dimensional filtered correlation $R(x^+, z^+ \mid \omega^+)$; $\omega^+ = 0{\cdot}0853$, $B_{np} = 0{\cdot}10$.

waves which can be sustained against the dissipative action of viscosity ($k^+_{\max} \approx 0{\cdot}05$). Ideally as large a range of wave sizes ($k^+_{\max}/k^+_{\min}$) as possible should be present in the flow without prejudicing the resolution of measurement. On this basis a friction velocity of 61·3 cm sec^{-1} provides a wave size range of 22 and was chosen for the measurements described. In addition it enabled direct comparisons to be made with the previous work of Morrison *et al.* (1969, 1971). Further, one expects that the waves of small inclination will have a maximum intensity for a critical layer constant $ky_c \approx 0{\cdot}6$ and so y_c was chosen from the geometric mean of the maximum and minimum permissible wave numbers ($y_c^+ \approx 55$). However, as some corrections due to wall effects could be expected at the calculated ($y^+ = 55$) position, measurements were taken for $y^+ = 70$ ($y = 1{\cdot}78$ mm, which is just on the limit of the wall-affected region). The flow Reynolds number was 69000 when calculated on the pipe radius and centre-line velocity.

The longitudinal velocity was measured with two linearized hot-wire anemometers (University of Queensland design) with tungsten wires of 5 μm diameter, 2 mm working length, and matched frequency response with a corner frequency of 25 kHz. The correlations – of which figures 3 and 4 are representative – were generated in narrow frequency bands at 160 Hz ($\omega^+ = 0{\cdot}0420$), 325 Hz ($\omega^+ = 0{\cdot}0853$) and 650 Hz ($\omega^+ = 0{\cdot}171$), with a heterodyne-type cross spectrum analyser, the correlations being normalized on the r.m.s. value of the filtered signals. Throughout this paper $R(x, z \mid \omega)$ and $R^\circ(x, z \mid \omega)$ are used to denote two point narrow-band correlations of the longitudinal velocity with zero time delay and 0° or 90° phase shift respectively. Filter total bandwidths (B_{np}) of 10 % ($\omega^+ = 0{\cdot}0420$ and $\omega^+ = 0{\cdot}0853$) and 5 % ($\omega^+ = 0{\cdot}171$) were used with a record length of 130 seconds per data point. To test the effect of filter

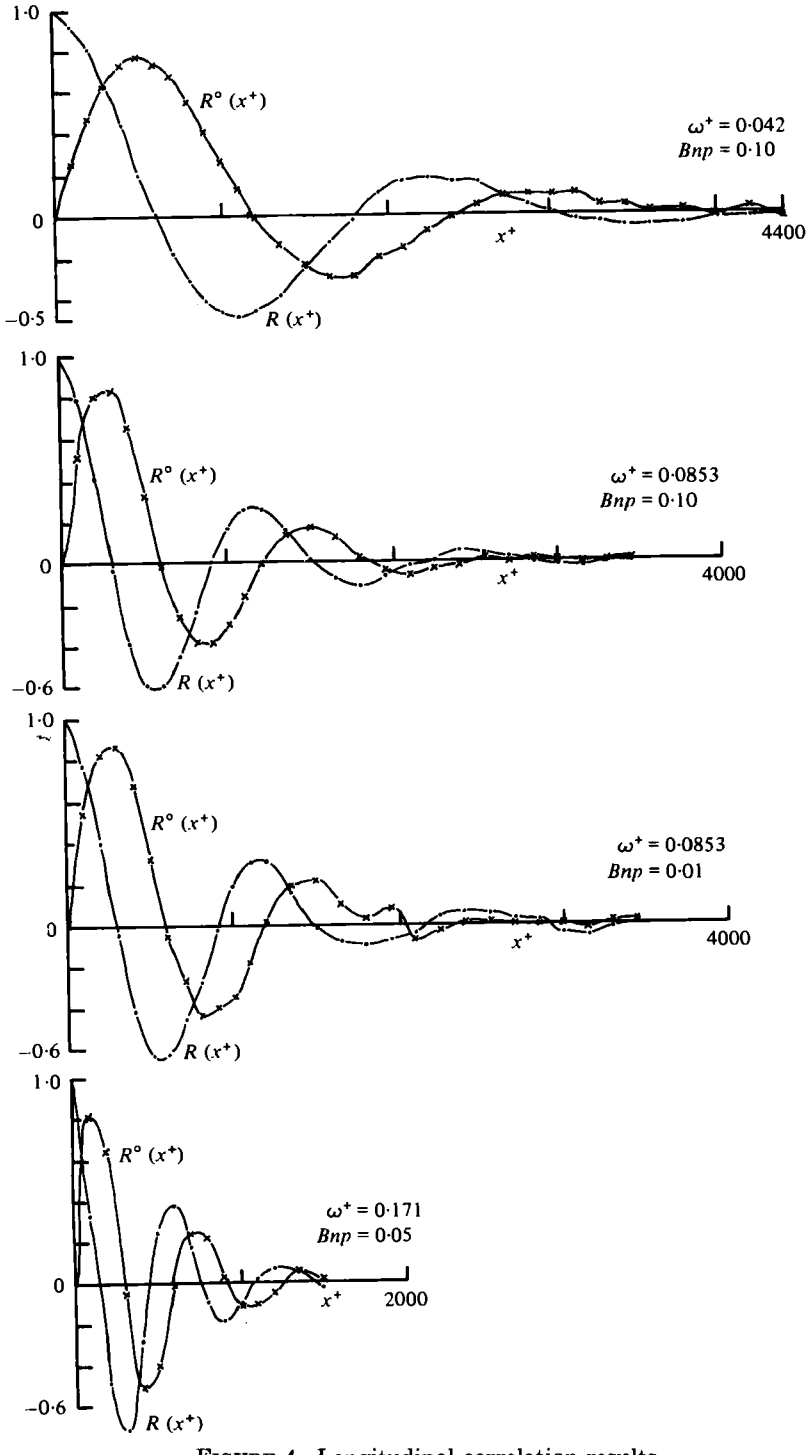

FIGURE 4. Longitudinal correlation results.

bandwidth, a 1 % half bandwidth filter was also used at $\omega^+ = 0{\cdot}0853$ with a record length of 130 seconds, however, the uncertainty in the correlations is correspondingly greater. Correlations were generated in this way for a total of 449 spatial separations up to a maximum longitudinal separation $x^+ = 4400$ (11·2 cm) and transverse separation $z^+ = 1100$ (24°). The longitudinal and transverse resolutions $\Delta x^+ = 100$ and $\Delta z^+ = 45{\cdot}7$ correspond to spatial Nyquist wavenumbers of $k_x^+ = 0{\cdot}32$ and $k_z^+ = 0{\cdot}070$.

Fourier transformation of the normalized filtered correlations was performed by linear interpolation between the measured values, thus allowing the contributions to the total integrals to be calculated analytically. Artificial 'correlation tails' were not added nor were the correlations smoothed before transformation. For homogeneous turbulent flow it is convenient to assume k_x is always positive and that sign variations occur in ω, so that wave propagation in the direction of the flow will be associated with opposite signs in ω and k_x. Percentage upstream propagation at any k_x is given by

$$\frac{\Phi(\omega, k_x)}{\Phi(\omega, k_x) + \Phi(-\omega, k_x)} = 0{\cdot}5 - \frac{\int_0^\infty R^\circ(x, 0 \mid \omega) \sin(k_x x)\, dx}{2\int_0^\infty R(x, 0 \mid \omega) \cos(k_x x)\, dx}. \tag{7}$$

Henceforth we will let $\Phi(\omega, k_x)$, $\Phi(\omega, k_z)$ and $\Phi(\omega, k_x k_z)$ represent the total energy of wave propagation, both upstream and downstream, with the spectral functions calculated as follows (the definitions for $\Phi(\omega, k_z)$ being omitted as they are similar to those for $\Phi(\omega, k_x)$):

$$\Phi(\omega^+, k_x^+) = \frac{2}{\pi}\int_0^\infty R(x^+, 0 \mid \omega^+) \cos(k_x^+ . x^+)\, dx^+,$$

$$\Phi(\omega^+, k_x^+, k_z^+) = \frac{2}{\pi^2}\int_0^\infty \int_0^\infty R(x^+, z^+ \mid \omega^+) \cos(k_x^+ . x^+) \cos(k_z^+ . z^+)\, dx^+ dz^+. \tag{8}$$

Normalization of the filtered correlations on the r.m.s. filtered signal has ensured that

$$\int_0^\infty \Phi(\omega^+, k_x^+, k_z^+)\, dk_z^+ = \Phi(\omega^+, k_x^+), \tag{9}$$

with integrals

$$\int_0^\infty \Phi(\omega^+, k_x^+)\, dk_x^+ = \int_0^\infty \Phi(\omega^+, k_z^+)\, dk_z^+ = 1{\cdot}0.$$

As pointed out by Morrison & Kronauer (1969) it is convenient to present the above spectra on logarithmic wavenumber scales so we define

$$P(\omega^+, k_x^+) = k_x^+ . \Phi(\omega^+, k_x^+), \quad P(\omega^+, k_x^+, k_z^+) = k_x^+ . k_z^+ . \Phi(\omega^+, k_x^+, k_z^+), \tag{10}$$

and observe that the integrals

$$\int_{-\infty}^\infty P(\omega^+, k_x^+)\, d(\ln k_x^+) = 1{\cdot}0, \quad \int_{-\infty}^\infty \int_{-\infty}^\infty P(\omega^+, k_x^+, k_z^+)\, d(\ln k_x^+)\, d(\ln k_z^+) = 1{\cdot}0$$

provide the correct normalization.

Table 1 lists the one-dimensional spectral functions, calculated percentage upstream propagation and the integrals in wavenumber space. Calculation of the propagation of

upstream propagation (7) requires very accurate estimates of the correlations $R^{\circ}(x, 0 \mid \omega)$ and $R(x, 0 \mid \omega)$ if meaningful results are to be obtained for regions of low spectral density in $P(\omega, k_x)$. This is well illustrated by the results for $\omega^+ = 0{\cdot}0853$ and filter half bandwidths of $B_{np} = 0{\cdot}10$ and $B_{np} = 0{\cdot}01$, and so the values are tabulated to correspond only with the more energetic longitudinal wavenumbers. The maximum upstream propagation is only 2 % ($\omega^+ = 0{\cdot}042$) (considering only that estimate corresponding to maximum spectral density of $P(\omega^+, k_x^+)$). Although the correlations measurements are being repeated to improve the accuracy, the present results would suggest that the energy associated with upstream wave propagation is negligible.

Fourier transforms $P(\omega^+, k_x^+, k_z^+)$ were first calculated for the wavenumbers k_x^+, k_z^+ shown in table 1 revealing that the contours were relatively localized in k_x^+, k_z^+ space. In addition these results show that areas of negative power spectral density existed – a physical impossibility which results from the measurement errors associated with finite length correlations, finite spatial sampling and the limited integration time for correlation at each data point. However it should be noted that the value of these negative regions is typically less than 5 % of the maximum $P(\omega^+, k_x^+, k_z^+)$ and unlikely to affect the shape of the two-dimensional transforms. A second set of transforms produced figures 5, 6 and 7 which show contour plots of $P(\omega^+, k_x^+, k_z^+)$ for various ω^+, each plot being computed for 25 equally spaced values in $\log k_x^+$ and $\log k_z^+$ (total of 625 spatial wavenumber points) over the range shown in the figures.

5. Interpretation and analysis of results

Contour plots of $P(\omega^+, k_x^+, k_z^+)$ for all frequencies chosen indicate that frequency filtering provides reasonable constraint on the longitudinal wavenumber k_z^+ but none of any significance on the transverse wavenumbers. Furthermore the integral projections $P(\omega^+, k_x^+)$ would appear to give reasonable estimates of the cross-sectional thickness of $P(\omega^+, k_x^+, k_z^+)$ at any k_z^+. In addition the longitudinal convection velocity appears to be significantly dependent on transverse wavenumber.

As the true transform $T(\omega^+, k_x^+, k_z^+)$ is sampled over the passband of the heterodyne filters, it is to be expected that the measured results $P(k_x^+, k_z^+)$ of figures 5, 6 and 7 may not give a true estimate of $T(\omega^+, k_x^+, k_z^+)$ at the centre frequency ω_0^+ of the filter. A method for estimating the effect of the filter bandwidth is as follows. The filtered transform $P(\omega^+, k_x^+, k_z^+)$ can be written as

$$\Omega_0 \Phi(\Omega_0)\, P(\Omega_0 K_x, K_z) \int_{-\infty}^{\infty} H(\Omega)\, d\Omega = \int_{-\infty}^{\infty} \Omega \Phi(\Omega)\, T(\Omega, K_x, K_z)\, H(\Omega)\, d\Omega \quad (11)$$

with $\Omega = \log_{10}(\omega/2\pi)$, $K = \log_{10} k$ and $H(\Omega)$ being the filter response function. In this formulation it must be remembered that $P(\omega, k_x, k_z)$ is normalized with respect to the frequency spectrum $\Phi(\omega)$ so that the absolute spectrum $\omega\Phi(\omega)\, P(\omega, k_x, k_z)$ (hereafter denoted by $\mathscr{P}(\omega, k_x, k_z)$) is required to estimate the true effect of finite filter bandwidths. Examination of the contour plots suggests that a suitable functional form for the true absolute spectrum $\Omega\Phi(\Omega)\, T(\Omega, K_x, K_z)$ would be

$$\Omega\phi(\Omega)\, T(\Omega, K_x, K_z) = f(K_z)\,(1 + \eta\Omega^1) \exp\{-(K_x^1 - \Omega^1)^2/2\sigma^2\}, \quad (12)$$

with

$$K_x^1 = K_x - K_0, \quad \Omega^1 = \Omega - \Omega_0$$

k_x^+	k_x^+ cosine transform	% upstream	k_z^+	k_z^+ cosine transform
	(1) $\omega^+ = 0{\cdot}0452$, $B_{np} = 0{\cdot}10$			
0·00100	0·0955	—	0·00099	0·0364
0·00112	0·1146	—	0·00132	0·0469
0·00127	0·1443	—	0·00174	0·0597
0·00143	0·1971	5·82	0·00230	0·0758
0·00162	0·2938	2·31	0·00305	0·0996
0·00183	0·4583	1·02	0·00403	0·1450
0·00206	0·6985	1·19	0·00532	0·2361
0·00233	0·9710	1·76	0·00704	0·3597
0·00263	1·1594	2·03	0·00930	0·4228
0·00297	1·1276	1·62	0·01230	0·4351
0·00335	0·8643	0·45	0·01625	0·4480
0·00379	0·5410	—	0·02148	0·3004
0·00428	0·3155	0·48	0·02839	0·2593
0·00483	0·1907	—	0·03753	0·1513
0·00545	0·1365	3·09	0·04960	0·0863
0·00615	0·0925	—	0·06555	0·0635
0·00695	0·0113	—	0·08663	0·0531
0·00784	0·0419	—	0·11450	0·0619
0·00885	0·0133	—	0·15132	0·0396
0·00999	0·0085	—	0·19999	0·2180
Integrals	0·9060	—	Integrals	0·9490
	(2) $\omega^+ = 0{\cdot}171$, $B_{np} = 0{\cdot}05$			
0·00399	0·0052	—	0·00099	0·0221
0·00451	0·0175	—	0·00132	0·0291
0·00509	0·0288	—	0·00174	0·0380
0·00575	0·0451	—	0·00230	0·0494
0·00649	0·1033	—	0·00305	0·0635
0·00733	0·2950	1·49	0·00403	0·0804
0·00827	0·7265	1·56	0·00532	0·1001
0·00934	1·3256	1·17	0·00704	0·1254
0·01054	1·6538	0·70	0·00930	0·1752
0·01190	1·3184	0·26	0·01230	0·2840
0·01343	0·7383	1·94	0·01625	0·3862
0·01517	0·3978	2·98	0·02148	0·4431
0·01712	0·1902	3·83	0·02839	0·4531
0·01933	0·1568	—	0·03753	0·3568
0·2182	0·1109	—	0·04960	0·2860
0·02463	0·0909	—	0·06555	0·1664
0·02780	0·1059	—	0·08663	0·1539
0·03139	0·0733	—	0·11450	0·0904
0·03543	0·0822	—	0·15132	0·0307
0·03999	0·0616	—	0·19999	0·0616
Integrals	0·9123	—	Integrals	0·9473
	(3) $\omega^+ = 0{\cdot}0853$, $B_{np} = 0{\cdot}10$			
0·00199	0·0432	—	0·00099	0·0312
0·00255	0·0690	—	0·00132	0·0397
0·00254	0·1076	—	0·00174	0·0495
0·00287	0·1592	—	0·00230	0·0602
0·00324	0·2371	—	0·00305	0·0729
0·00366	0·3971	—	0·00403	0·0952
0·00413	0·7263	—	0·00532	0·1464
0·00467	1·1883	0·62	0·00704	0·2373

k_x^+	k_x^+ cosine transform	% upstream	k_z^+	k_z^+ cosine transform
0·00527	1·4623	0·53	0·00930	0·3283
0·00595	1·2715	—	0·01230	0·4047
0·00671	0·8489	0·19	0·01625	0·4509
0·00758	0·4793	—	0·02148	0·4418
0·00856	0·2282	—	0·02839	0·3642
0·00966	0·1418	—	0·03753	0·2315
0·01091	0·0520	—	0·04960	0·1166
0·01231	0·0740	—	0·06555	0·0849
0·01390	0·0333	—	0·08663	0·0692
0·01569	0·0725	—	0·11450	0·0873
0·01771	0·0097	—	0·15132	0·0392
0·01999	−0·0034	—	0·19999	0·0241
Integrals	0·9209	—	Integrals	0·9414
	(4) $\omega^+ = 0{\cdot}0853$, $B_{np} = 0{\cdot}01$			
0·00199	0·0188	—	0·00099	0·0264
0·00255	0·0434	—	0·00132	0·0343
0·00254	0·0834	—	0·00174	0·0441
0·00287	0·1365	—	0·00230	0·0562
0·00324	0·2095	—	0·00305	0·0725
0·00366	0·3585	—	0·00403	0·0989
0·00413	0·6987	—	0·00532	0·1493
0·00467	1·2240	16·14	0·00704	0·2350
0·00527	1·5413	14·29	0·00930	0·3296
0·00595	1·2947	15·96	0·01230	0·3968
0·00671	0·9016	37·99	0·01625	0·4650
0·00758	0·4850	—	0·02148	0·4678
0·00856	0·1547	—	0·02839	0·4237
0·00966	0·1325	—	0·03753	0·2071
0·01091	0·2191	—	0·04960	0·1270
0·01231	0·0028	—	0·06555	0·1115
0·01390	0·0555	—	0·08663	0·0792
0·01569	0·0899	—	0·11450	0·0904
0·01771	0·0776	—	0·15132	0·0399
0·01999	0·1486	—	0·19999	0·0325
Integrals	0·9546	—	Integrals	0·9727

TABLE 1. One-dimensional wave spectra

Ω_0 being the logarithm of the filter centre frequency, K_0 the mean value of the distribution in K_x, and σ^2 the variance of the distribution. The slope parameter η allows for variation in spectral power with frequency. Solution of the above equations simultaneously (with the expressions for filter response $H(\Omega)$) allows values of K_0, σ^2 and $f(K_z)$ to be fitted to the experimental data points by use of a Marquardt multivariable optimization routine (Kuester & Mize 1973).

The results when corrected for filter bandwidth showed negligible variation (within the accuracy of the data) from the measured transforms of figures 5–7, thus indicating that the bandwidth of the filters was small enough. While $P(\omega, k_x, k_z)$ is not presented for $\omega^+ = 0{\cdot}0853$ and $B_{np} = 0{\cdot}01$, it was calculated and compared with the presented results for $B_{np} = 0{\cdot}10$. Observed differences were slight, and even though the two results are of quite different accuracies this again demonstrated that filter bandwidth

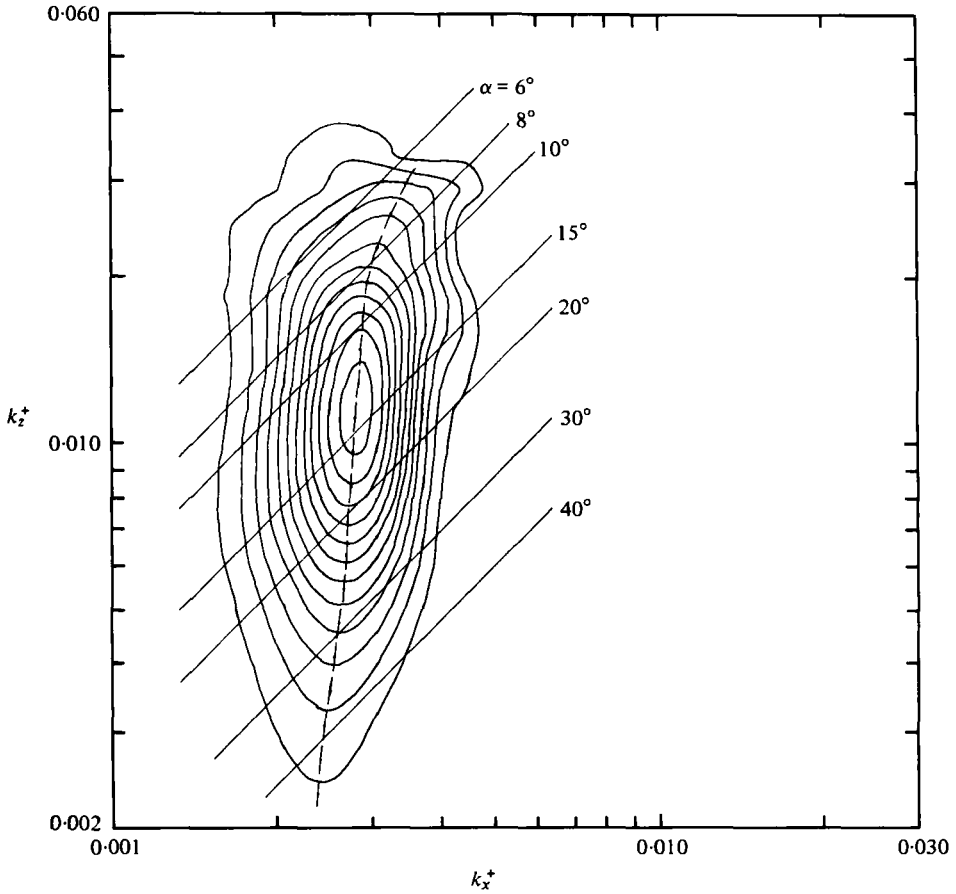

FIGURE 5. Contours of two-dimensional power spectral density. $P(\omega^+, k_x^+, k_z^+)$; $\omega^+ = 0{\cdot}042$, $B_{np} = 0{\cdot}10$. Maximum contour $-0{\cdot}65$; contour interval $-0{\cdot}05$.

effects were negligible. Also calculated were the percentage half bandwidths B_{kp} of spatial filters corresponding to the half-power points in k_x of experimental data fitted by (12) for particular k_z and ω. Figure 8 presents a contour plot of B_{kp}as a function of wave inclination and wavenumber deduced from the ridge lines shown in figures 5, 6 and 7. The data points of the ridge lines are shown for the three ω^+ under consideration, but not the values of B_{kp} which of course enable the contours to be drawn.

Corresponding to the average half bandwidth ($B_{kp} = 0{\cdot}25$) one would expect to see a full length of 4π radians, or 2 wavelengths, in a typical wave packet of fixed wavenumber and inclination. Remembering that it is possible for individual members of the ensemble to have larger coherence lengths than the above, the use of the wave model proposed would seem to be relatively justified – especially when one recalls that in signal processing terminology filters of 20 % half bandwidth are usually considered as being narrow. Further the results of figures 5, 6 and 7 indicate that the integral projections $P(\omega, k_x)$ give only reasonable estimates of the thickness of $P(\omega, k_x, k_z)$ at any k_z^+ because of the significant curvature in the ridge lines of these plots at high values of k_z^+.

Estimation of the convection velocity associated with a particular wavenumber

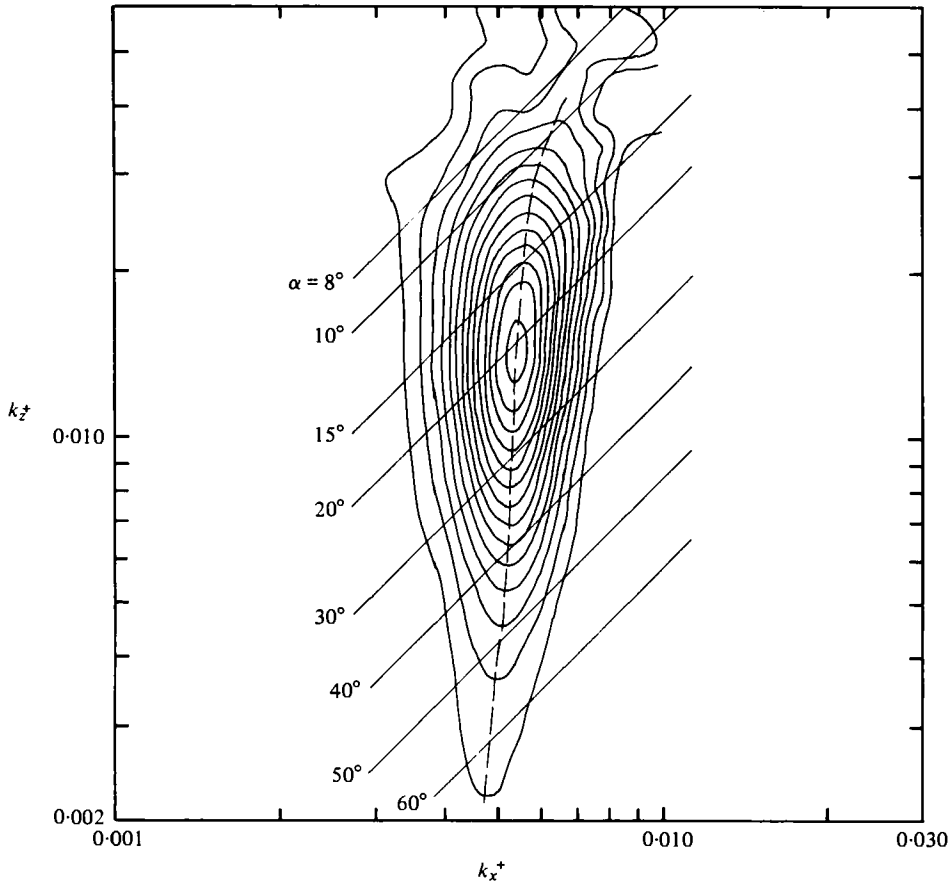

FIGURE 6. Contours of two-dimensional power spectral density. $P(\omega^+, k_x^+, k_z^+)$; $\omega^+ = 0{\cdot}0853$, $B_{np} = 0{\cdot}10$. Maximum contour $-0{\cdot}75$; contour interval $-0{\cdot}05$.

and inclination is best performed by examining the variation in $\mathscr{P}(\omega^+, k_x^+, k_z^+)$ for fixed k_x^+ and k_z^+. As indicated by (4) this variation will be symmetric in ω^+ about that frequency ω^+ corresponding to the mean convection velocity. Unfortunately this information does not exist as it represents an enormous volume of experimentation, and so we must resort to estimating convection velocity from the measured transforms of figures 5, 6 and 7.

We approach the problem by determining the locus of the ridge line of $P(\omega, k_x, k_z)$ for each frequency and equate this to the variation in mean convection velocity with wavenumber and angle of inclination. Equations (11) and (12), while useful in determining the wave coherence lengths, will provide a biased estimate of this ridge line such bias resulting from an optimization scheme in a plane non-orthogonal to the local direction of the ridge line. Longitudinal convection velocities were determined from the location of these ridge lines (figures 5, 6 and 7) and the results of the wavenumber dependence are shown in figure 9 in addition to some contours of constant wave inclination α. The positions of the ridge lines were determined by inspection on large scale contour plots, and the results obtained independently by five colleagues were compared – the total variability was less than 1 % for these manually determined ridge lines.

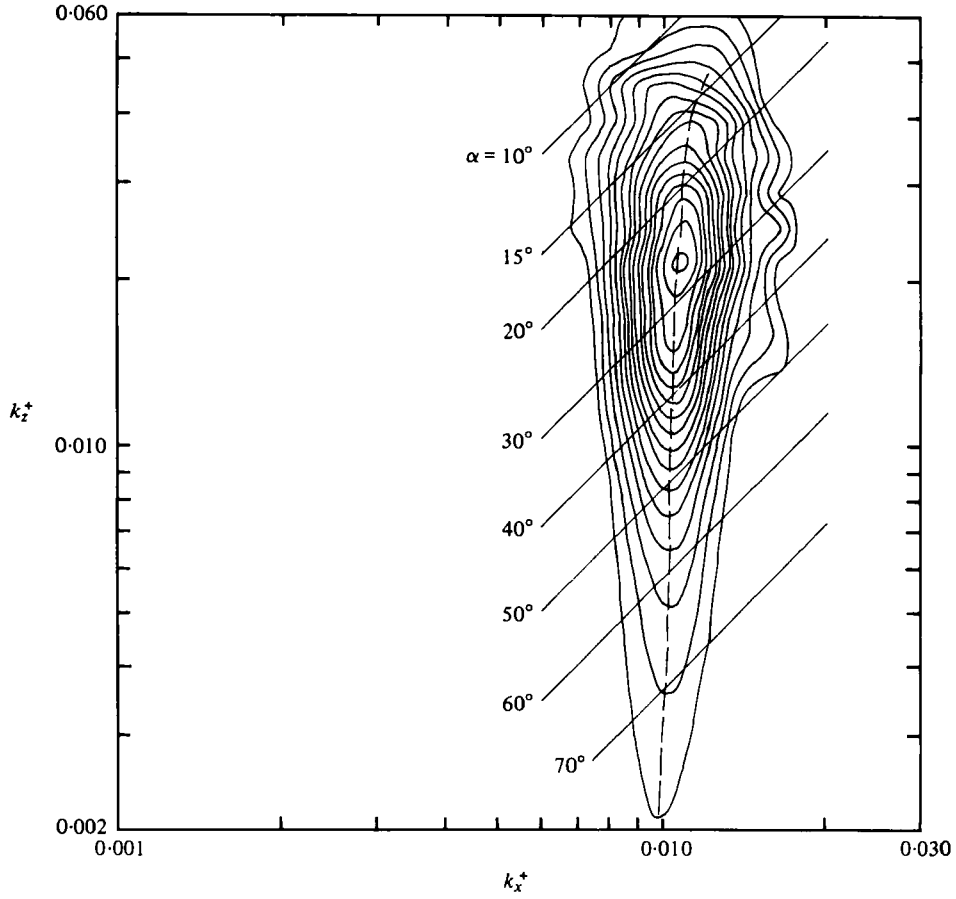

FIGURE 7. Contours of two-dimensional power spectral density. $P(\omega^+, k_x^+, k_z^+)$; $\omega^+ = 0{\cdot}171$, $B_{np} = 0{\cdot}05$. Maximum contour $-0{\cdot}85$; contour interval $-0{\cdot}05$.

Figure 9 is at variance with the predictions of Morrison & Kronauer (1969) in two ways for waves of extent large with respect to the wall layer ($y^+ \simeq 70$), and for which (6) was expected to apply. Firstly, there is a strong frequency dependence in the value of β to satisfy (6) and secondly the calculated points for $C_x^+ \geqslant 16$ and $\omega^+ = 0{\cdot}171$ would not appear to satisfy adequately the functional form of (6). However the ridge line data for the three frequencies would seem to collapse well if the restriction on a logarithmic profile is relaxed, and the convection velocities plotted as $C_x^+(k^+/S(\omega^+)$ as shown in figure 10 – where $S(\omega^+)$ has been chosen to have the following values

$$S(0{\cdot}042) = 0{\cdot}59, \quad S(0{\cdot}0853) = 1{\cdot}00, \quad S(0{\cdot}171) = 1{\cdot}60.$$

In addition figure 10 provides collapse of the ridge line data irrespective of wave inclination and while there is a variability in the collapse for the range $16{\cdot}5 < C_x^+ < 14{\cdot}0$ all results are within $\pm 2\,\%$ of the average over the whole decade of wavenumbers investigated. Introduction of the $S(\omega)$ term to collapse the data in figure 10 indicates that the approach of Morrison & Kronauer in assuming geometrical scaling of the critical layer is incorrect. The bracketed values of y^+ in figure 10 represent the distance

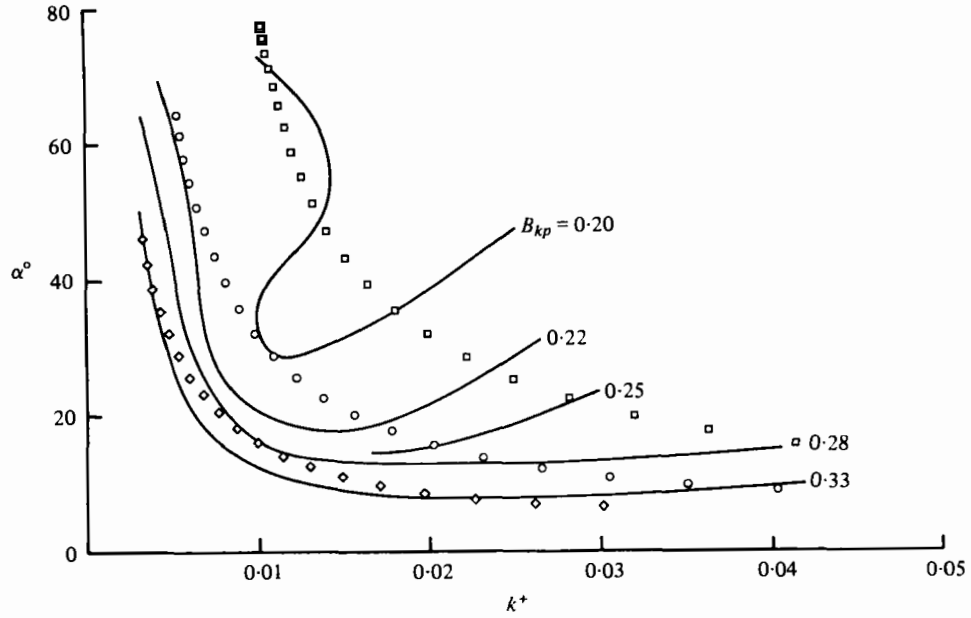

FIGURE 8. Wavenumber percentage half bandwidth contours.
◇, $\omega^+ = 0{\cdot}042$; ○, $\omega^+ = 0{\cdot}0853$; □, $\omega^+ = 0{\cdot}171$.

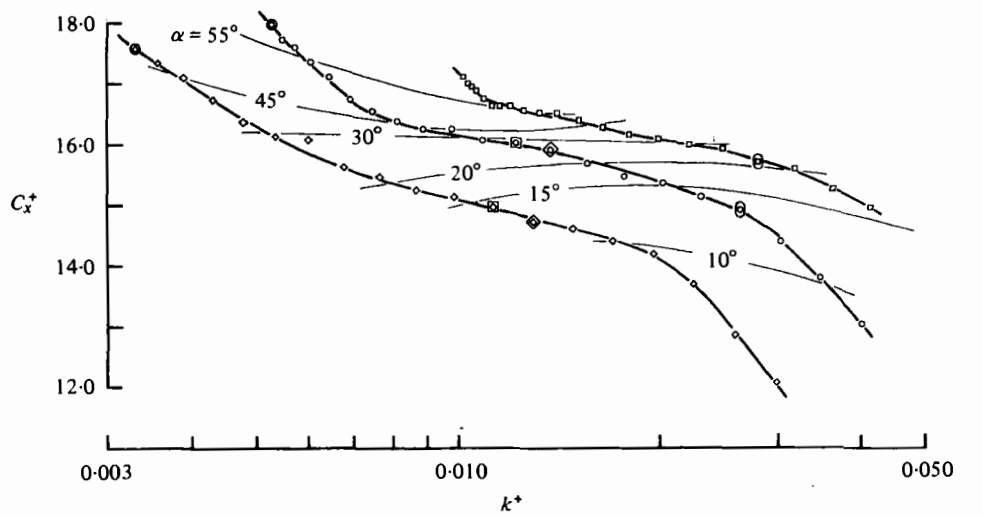

FIGURE 9. Dependence of mean convection velocity on wavenumber. ◇, $\omega^+ = 0{\cdot}042$; ○, $\omega^+ = 0{\cdot}853$; □, $\omega^+ = 6{\cdot}171$. ◎, ◎, $k_z^+ = 0{\cdot}0023$; ⊡, ⊡, $k_z^+ = 0{\cdot}0118$; ◈, ◈, $k_z^+ = 0{\cdot}0137$; ⊖, ⊖, $k_z^+ = 0{\cdot}0288$.

from the wall at which the mean velocity profile U^+ corresponds to values of convection velocity C_x^+ shown on the figure.

For the constant-stress region of the turbulent boundary layer on a rough or smooth wall the assumption that the local values of Reynolds stress, energy dissipation and lateral flux of turbulent energy depend only on wall stress and distance from the wall

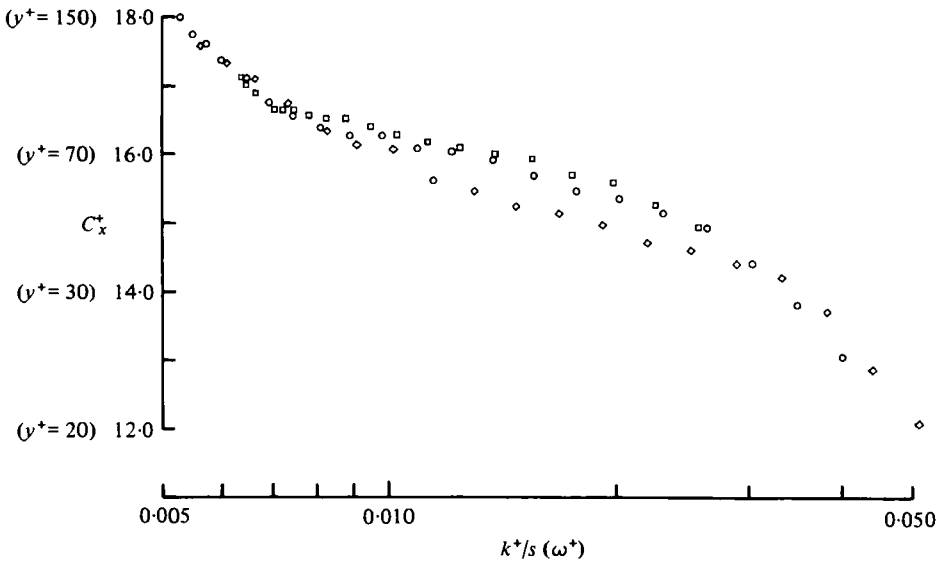

FIGURE 10. Dependence of mean convection velocity on modified wavenumber. ◇, $\omega^+ = 0{\cdot}042$; ○, $\omega^+ = 0{\cdot}0853$; □, $\omega^+ = 0{\cdot}171$.

leads to the logarithmic form of the mean velocity distribution. The choice of a geometrically similar wave model, which satisfies the flow continuity equations, is one model capable of generating the correct form of Reynolds stress, dissipation scales and lateral fluxes of turbulent energy in this region of logarithmic mean velocity profile. However it is difficult to see how the absolute speed of wave propagation is a property of geometric similarity *per se*. Rather it would appear that the convection velocity of a particular wave is determined from the Navier–Stokes equation for that wave, and so is strongly dependent on the mean velocity profile and the energy interchange from other waves in the flow. Morrison & Kronauer (1969) quite rightly indicate that for fully-developed turbulent flow it is the nonlinear terms which assume importance at the critical layer, however this should not be interpreted as necessitating constraint of the energy exchange process to select only those waves with convection velocities satisfying geometric scaling of the critical layer.

The results of Bullock *et al.* (1978) provide no experimental measure of k_x or k_z for their filtered correlations normal to the wall. As such they inferred k_x from the filtering frequency ω and elected to ignore any angular variation due to a spread on k_z for that frequency. Hence the data collapse with $k_x y$ does not rigorously indicate similarity of streamlines in the total wavenumber sense (that is with ky). However their similarity curves do collapse the data for a frequency range of 6 to 1 and so tend to support a wave model with no geometric constraint of the critical layer.

Figures 9 and 10 are derived on the basis that the ridge of $P(\omega, k_x k_z)$ gives a true estimate of the convection velocity $C_x(k, \alpha)$. If one plots now the absolute spectrum $P(\omega, k_x, k_z)$ against ω and k_x for fixed k_z, it will be apparent that there is a variation in power of these contours from low to high k_x. Alternatively we say that in terms of (12) the slope parameter η is in general non-zero. Hence one would expect that determination of convection velocity by holding ω and k_z constant will in general give a different result than an optimization with k_z and k_x constant – the difference in

estimate being a function of the slope parameter η. Furthermore if the slope parameter η is zero at the k_z under investigation both optimization schemes will yield identical results, and the ridge line method (on which figures 9 and 10 were derived) will give an unbiased estimate of the convection velocity $C(k, \alpha)$ for those k_z where $\eta = 0$.

At each k_z the maximum value of $P(\omega, k_x, k_z)$ at the three experimental frequencies was determined and plotted against the value of k_x corresponding to this maximum. The curves were normalized to unity at $\omega^+ = 0{\cdot}0853$ and interpolated by a quadratic in k_x – the derivative of which is an estimate of the slope parameter η. Examination of these curves at $\omega^+ = 0{\cdot}042$ showed that all values lay in the range 0·7 to 1·8 with the values for $k_z^+ = 0{\cdot}0023$ and $0{\cdot}0118 \leqslant k_z^+ \leqslant 0{\cdot}0137$ lying in the range 0·9 to 1·10 and exhibiting negligible slope parameter η. Hence we would expect that these sections of the ridge line should provide an unbiased estimate of the convection velocity for both $\omega^+ = 0{\cdot}042$ and $\omega^+ = 0{\cdot}0853$. Similarly for $\omega^+ = 0{\cdot}0853$ and $\omega^+ = 0{\cdot}171$ this applies for $0{\cdot}0248 \leqslant k_z^+ \leqslant 0{\cdot}0334$, although the curvature of the ridge lines with high k_z (figures 5, 6 and 7) must cast doubt on the strict applicability of this reasoning at these large values of k_z. For reference some values of k_z^+ (and hence k^+) corresponding to $\eta = 0$ have been marked on figure 9. From these results it is inferred that figures 9 and 10 support the data collapse as $C_x^+(k^+/S(\omega^+))$ with no bias for those k_z^+ where $\eta = 0$, and it is believed that the non-zero slope parameter will not significantly effect the other data points for the k_z^+ range under investigation.

The collapse of figure 10 is equivalent to plotting wave convection velocity C_x^+ as a function of wave critical layer height y_c^+. In their derivation of (6), Morrison & Kronauer (1969) effectively assumed that the wave height (and hence y_c^+) was large when compared with the dimensions of the wall region ($y^+ \leqslant 70$). As such one might expect their functional form (when modified to include the $S(\omega)$ term) to apply for higher convection velocities, e.g. $C_x^+ > 18$, but unfortunately in the present experiment the Reynolds number was too low and the filtering frequencies too high to guarantee a significant region at higher convection velocities. For waves with critical layer dimensions comparable to those of the wall layer, one would expect viscosity to play a significant part in the generation of the wave stream functions h_1 and h_2. However the collapse of figure 10 appears adequate to wave convection velocities above $C_x^+ = 12$ (corresponding to a distance from the wall $y^+ \geqslant 20$ from the universal velocity profile).

No attempt has been made to correlate the percentage half bandwidths B_{kp} as the contour plots of figures 5, 6 and 7 indicate that for high k_z^+ (and relatively high curvature in the ridge lines with k_x^+ and k_z^+), the percentage half bandwidth B_{kp} will give an erroneous estimate of the spectral spread in ω^+ for a wave of fixed inclination and wavenumber (as B_{kp} is determined in a plane non-orthogonal to that of maximum power gradient in ω^+). Direct measurement of the variation in ω^+ at fixed k^+ and α will provide the associated distribution in convection velocity and such a project is under investigation at present.

In evaluating the results overall we should re-examine the flow conditions chosen in the design of the experiment. From the contour plots of figures 5, 6 and 7 and the ridge line data of figure 9 it is obvious that the more energetic waves are spread over the range

$$6{\cdot}6^\circ < \alpha < 77^\circ, \quad 0{\cdot}0033 < k^+ < 0{\cdot}0415, \quad 0{\cdot}23 < k^+ y^+ < 2{\cdot}90.$$

As such a reasonable range of wave sizes ($k_{\max}^+/k_{\min}^+ = 12{\cdot}6$) has been covered although

this could have been extended to lower k^+ by choice of lower filter frequencies, and to higher k^+ by the use of higher Reynolds numbers. Similarly the choice of the measurement station at $y^+ = 70$ rather than further out in the flow has selected the smaller wavelength components in the flow on an intensity basis, whereas measurement further out would have selected the longer wavelength components and allowed investigation of the higher C_x^+ regime of figure 10. However as one would expect the longer wavelength components to be less affected by viscous effects, the choice of $y^+ = 70$ has indicated more strongly the potential of a geometrically similar wave model for collapsing the results of boundary layer turbulence.

6. Conclusion

The paper presents the first measurements, to the author's knowledge, of the three-dimensional power density distribution function $\Phi_{uu}(k_x, k_z, \omega)$, i.e. the Fourier transform of the cross-correlation function $R_{uu}(\Delta x, \Delta z, t)$ at a fixed y^+ distance of 70. The postulate of Morrison & Kronauer (1969) of a similarity variable ky scaling the location of the critical layer is tested and found to be unsatisfactory. With the introduction of a modified variable $C_x^+(k^+/S(\omega^+))$ the convection velocity appears to be independent of the wave propagation angle α even though the power is distributed over a wide range of α, viz. 7–77°.

The critical layer for waves of reasonable intensity as measured at the y^+ station of 70 covers a y^+ range of 20–150 corresponding to a U^+ of 12 to 18. The smallest wavelength of turbulence with significant energy at $\omega^+ = 0{\cdot}171$ is $\lambda^+ = 150$ while the largest wavelength measured at the lower frequency $\omega^+ = 0{\cdot}042$ is $\lambda^+ = 1990$, which is very close to the equivalent y^+ of the centre of the tube, viz. 2600.

The data demonstrate that the thickness of the sheet on which the energy of the u component is located in ω, k_x, k_z space is relatively thin and that the bandwidth associated with u turbulence is relatively undamped possessing a coherence length for a wave packet of at least $1\frac{2}{3}$ wavelengths.

This extensive but nevertheless preliminary experiment provides the justification for pursuing a more detailed and larger investigation at defined y_1, y_2 locations to determine the exact form of the h_1, h_2 functions for the velocity components, as well as investigating the convection velocity dependence over a larger range of wave parameters.

Professor R. E. Kronauer, of Harvard University and Professor K. J. Bullock, of University of Queensland, have both contributed greatly by their many personal communications and discussions on the wider aspects of this work.

The financial support of both the Australian Research Grants Committee and the Australian Institute of Nuclear Science and Engineering in helping to provide the special research facilities used in this investigation are gratefully acknowledged.

REFERENCES

BULL, M. K. 1967 *J. Fluid Mech.* **28**, 719.

BULLOCK, K. J., COOPER, R. E. & ABERNATHY, F. H. 1978 *J. Fluid Mech.* **88**, 585.

CRAIK, A. D. D. 1971 *J. Fluid Mech.* **50**, 393.

ELLIOTT, J. A. 1972 *J. Fluid Mech.* **53**, 351.

FAVRE, A. J., GAVIGLIO, J. J. & DUMAS, R. J. 1957 *J. Fluid Mech.* **2**, 313.

FAVRE, A. J., GAVIGLIO, J. J. & DUMAS, R. J. 1958 *J. Fluid Mech.* **3**, 344.

GRANT, H. L. 1958 *J. Fluid Mech.* **4**, 149.

KOVASZNAY, L. S. G., KIBENS, V. & BLACKWELDER, R. F. 1970 *J. Fluid Mech.* **41**, 283.

KUESTER, J. L. & MIZE, J. H. 1973 *Optimization Techniques with Fortran.* McGraw-Hill.

LAUFER, J. 1954 *N.A.C.A. Rep.* no. 1174.

LUMLEY, J. L. 1967 Proceedings of the International Colloquium on the Fine Scale Structure of the Atmosphere and its Influence on Radio Wave Propagation. *Dokl. Akad. Nauk S.S.S.R. Moscow.*

MCCONACHIE, P. J. 1975 The structure of turbulence in shear flows. Ph.D. thesis, Department of Mechanical Engineering, University of Queensland, Australia.

MORRISON, W. R. B., BULLOCK, K. J. & KRONAUER, R. E. 1971 *J. Fluid Mech.* **47**, 639.

MORRISON, W. R. B. & KRONAUER, R. E. 1969 *J. Fluid Mech.* **39**, 117.

TOWNSEND, A. A. 1956 *The Structure of Turbulent Shear Flow.* Cambridge University Press.

TOWNSEND, A. A. 1958 Boundary Later Research Symposium, International Union of Theoretical and Applied Physics. Springer, Berlin.

TOWNSEND, A. A. 1976 *The Structure of Turbulent Shear Flow*, 2nd edition. Cambridge University Press.

WILLMARTH, W. W. & WOOLRIDGE, C. E. 1962 *J. Fluid Mech.* **14**, 187.